Fast Flow-Line-Based Analysis of Ultrasound Spectral and Vector Velocity Estimators

Jørgen Avdal, *Member, IEEE*, and Ingvild Kinn Ekroll, and Hans Torp, *Member, IEEE*

Abstract—A new technique, termed FLUST (FlowLine Ultrasound Simulation Tool), is proposed as a computationally cheap alternative to simulations based on randomly positioned scatterers for the simulation of stationary blood velocity fields. In FLUST, the flow field is represented as a collection of flow lines. Point spread functions are first calculated at regularly spaced positions along the flow lines before realizations of single scatterers traversing the flow lines are generated using temporal interpolation. Several flow-line realizations are then generated by convolution with temporal noise filters, and finally, flow-field realizations are obtained by the summation of the individual flow-line realizations. Flow-field realizations produced by FLUST are shown to correspond well with conventional Field II simulations both quantitatively and qualitatively. The added value of FLUST is demonstrated by using the proposed simulation technique to obtain multiple realizations of realistic 3-D flow fields at a significantly reduced computational cost. This information is utilized for a performance assessment of different spectral and vector velocity estimators for carotid and coronary imaging applications. The computational load of FLUST does not increase substantially with the number of realizations or simulated frames, and for the examples shown, it is the fastest alternative when the total number of simulated frames exceeds 48. In the examples, the standard deviation and bias of the velocity estimators are calculated using 100 FLUST realizations, in which case the proposed method is two orders of magnitude faster than simulations based on random scatterer positions.

Index Terms—Blood flow measurement, medical imaging, simulation.

I. INTRODUCTION

DOPPLER ultrasound is an important diagnostic tool used both for the detection and visualization of blood flow and the quantification of velocities. Color flow imaging (CFI) techniques provide the estimates of mean blood velocities in a large region of interest, which is useful for the navigation and detection of areas with high-velocity flow. Complementary to CFI is pulsed-wave (PW) and continuous-wave Doppler, spectral Doppler techniques that provide the distribution of blood velocities over time, currently used to estimate maximum velocities in stenotic regions or insufficiencies in the heart [1]. In recent years, increasing memory capacity and computational power of ultrasound systems has enabled blood flow imaging in 2-D or 3-D at high temporal resolution, using estimators

based on, e.g., triangulation of Doppler measurements [2]–[6], transverse oscillations [7], [8], or cross correlation of RF or baseband signals [9]–[13].

Both conventional Doppler and vector velocity techniques are prone to estimation errors. As an example, conventional CFI uses the autocorrelation estimator, which produces biased estimates when applied to clutter filtered data [14]. The autocorrelation estimate is also prone to variance depending on the bandwidth of the Doppler signal and variation in the center frequency of the backscattered signal.

Because of such challenges, new velocity estimation techniques need to be validated extensively before they can be used for diagnostic purposes, especially if they are to be used for quantitative measurements. Ideally, a method should have a strong theoretical foundation, be validated through simulations, and show consistent and promising results in flow phantoms and *in vivo*.

A common method for validating the velocity estimators in simulations is to generate synthetic data sets using ultrasound simulation software. By applying velocity estimators to simulated data, it is possible to quantify the statistical properties of the estimators, for example, the bias. However, both mean velocity estimators and spectral estimators used in ultrasound typically have high variance, meaning that several realizations of the flow field are necessary to reliably quantify the estimator properties. Field II [15], [16] is widely used to generate synthetic data sets, as it is known to be accurate in the linear domain. However, in order to obtain valid speckle statistics of the received signal, approximately 10 scatterers per resolution cell are needed [17]. As the simulation time scales with the number of scatterers, running a sufficiently large number of realizations for large and complex flow fields can be time-demanding. To avoid unreasonably long simulation times, evaluation of an estimator's performance is often based on single realizations of the flow field, using spatial averaging to reduce variance [3], [18], [19]. As a result, bias and variance of the applied estimator cannot be truly evaluated.

Reduced computational cost can be obtained by using different methods for calculating the spatial impulse response. The software Fast Ultrasound Simulation in K-Space (FUSK) [20] operates in the frequency domain and has been shown to reduce the simulation time by three orders of magnitude compared with Field II. However, as the PSF in FUSK is estimated based on the Fraunhofer approximation, realistic speckle statistics is only obtained in the focal region. COnvolution LEuven (COLE) [21] operates in the spatio–temporal domain, and is faster than FUSK when simulating
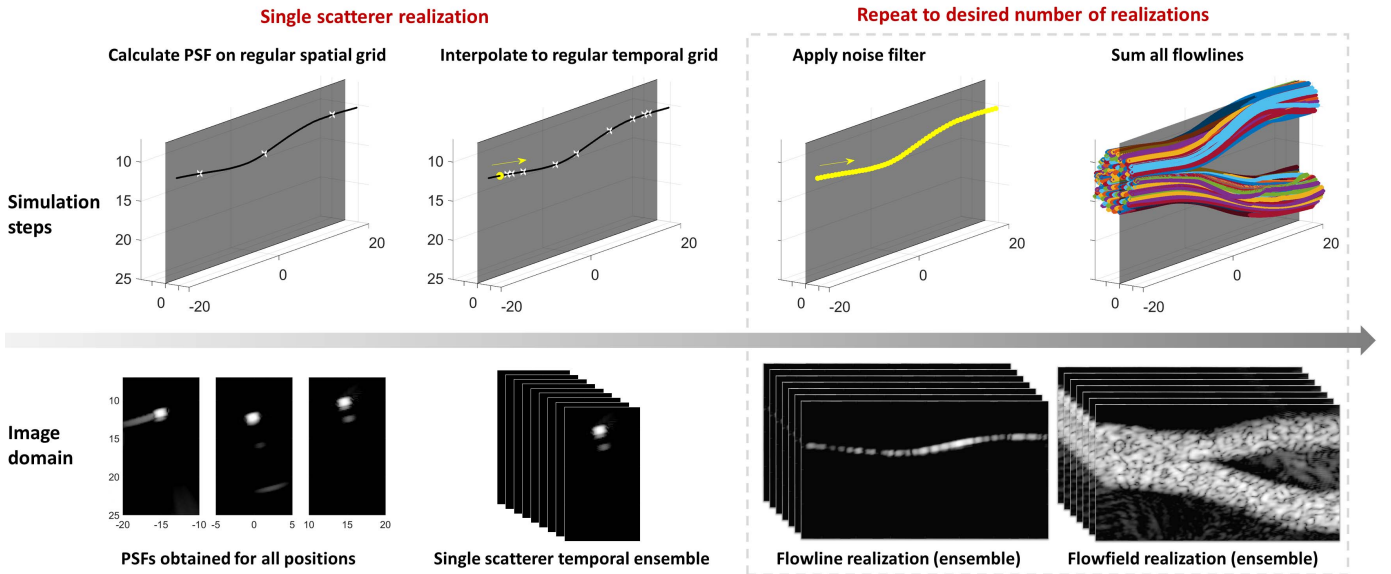
Fig. 1.   Stepwise illustration of FLUST: For a given flow line, PSFs are calculated for each scatterer position (using Field II or alternative tools). The signal from a single scatterer over the observation window is obtained by interpolation to a temporal grid. In the next step, a temporal noise filter is applied to obtain the signal from multiple scatterers moving along the flow line, yielding a single flow-line realization. To produce a full flow-field realization, the signal from all flow lines are summed. By repeating the two last steps, the desired number of ensemble realizations can be obtained at a low computational cost.

image sequences [22]. Measured beam profiles can be used to obtain more realistic image properties using lookup tables, but the PSF is still assumed separable. A graphical processing unit (GPU) version of COLE has also been implemented, reporting a speedup of 27 000 compared with multithreaded Field II simulations [23]. A different approach is taken in Fast And Mechanical Ultrasound Simulation (FAMUS) [24], where it is assumed that the field due to a sufficient number of point sources/receivers on the transducer surface is a good approximation to that produced by a real transducer. The method is inherently parallelizable, and a recently proposed modification of the method was shown to be two orders of magnitude faster than Field II [25].

In this paper, we propose an alternative simulation method for calculating the statistical expectation value and the variance of a velocity estimator when applied to *in silico* flow fields. The proposed method, which we term FLUST (FlowLine Ultrasound Simulation Tool), decomposes the flow field into flow lines rather than individual point scatterers. We will demonstrate that this allows us to estimate, with good accuracy, the expectation value and variance of velocity estimators faster than what would be possible with simulations based on randomly placed scatterers. Because the true velocities in the flow field are known in simulations, this produces an accurate quantitative assessment of the performance of the estimator. Such a tool is useful for the quantitative evaluation and optimization of estimators and comparison between different estimators.

This paper is organized as follows. Sections II-A and II-B explain the FLUST simulation technique. Section III describes the investigated velocity estimators, whereas Section IV describes the different simulation scenarios. To motivate the use of FLUST and validate its output, 3-D parabolic blood flow in a straight vessel is used. Models with more complex 3-D flow, a carotid artery bifurcation, and stenotic coronary arteries were used to demonstrate how FLUST enables the performance comparison of different vector and spectral estimators in realistic flow fields at a low computational cost. Results are found in Section V, discussion in Section VI, and conclusion in Section VII.

II. FLUST SIMULATION METHOD

The FLUST method produces multiple realizations of the received ultrasound signal from a stationary flow field. The method may be described as consisting of four main steps: 1) representing the flow field as a collection of flow lines; 2) calculating the received signals from single scatterers moving along each of the flow lines; 3) generating the received signal from a collection of scatterers moving along each flow line; and 4) summing the received signals from all flow lines. The steps of the FLUST method are summarized in Fig. 1 and Table I and are further detailed in the following.

A. Flow-Line Generation

The original velocity fields were described using an analytic expression, for fluid in a straight tube, or numerically as velocities on a selection of spatial points, for CFD simulations of more complex geometries. Flow lines were generated from the velocity field using two steps. First, a collection of seed points was selected, forming a rectangular grid with a resolution 0.5 mm on a cross section of the flow phantom. Then, one flow line was generated from each seed point by forward and backward propagation in time, using the velocity field and finite difference methods. Propagation was terminated when the lines crossed exit planes surrounding the phantom or left the region with valid velocities. The resulting flow lines are represented in the following mathematical form as $\mathbf{r}_F(t)$, denoting the position of a scatterer along the flow line F at time t. To minimize the number of flow lines leaving the

---

Parameters: Seed point grid resolution ΔS, PSF spacing Δd.

FLUST steps:

    1 Seed point grid generation:
- Select 2-D cross-section through phantom.
- Generate seed point grid with spacing ΔS.

    2 Flow line generation: for every flow line,
- select point from seed point grid .
- propagate forward and backward from seed point.

    3 Single scatterer ensemble realization: for every flow line,
- calculate PSFs along flow line with spacing Δd.
- interpolate to regular temporal grid.

    4 Multiple scatterers ensemble realization (noise filter): for every flow line,
- Fourier transform (single scatterer) signal.
- multiply with noise and displacement factor
- inverse Fourier transform

    5 Flowfield realization:
- Sum multiple scatterer realization from all flow lines

    6 Multiple flowfield realizations:
- Repeat step 4 and 5 to desired number of realizations

---

region containing valid velocities, the cross section containing seed points was placed downstream from the main bifurcations in the more complex geometries shown in this paper.

B. Generating Single Scatterer Realizations

Using the simulation software Field II, point spread functions (PSFs) were calculated for scatterer positions along F, as shown in the second column of Fig. 1. In this paper, the PSFs were calculated for positions evenly distributed along the flow line with a distance 0.05 mm, corresponding to one-sixth of a wavelength for the highest frequencies used. This density was selected such that the PSFs at all points along the flow line could subsequently be obtained by interpolation without a significant interpolation error. The calculated PSFs are dependent on the transducer geometry, pulse excitation, beamforming setup, and parameters that are specific to each application and specified in Section IV.

Using these PSFs and the flow-line function $\mathbf{r}_F$, we defined a function h_F of time and space describing the received signal from a single scatterer moving along F, by using the relation

$$h_F(\mathbf{r}, t) = \text{PSF}(\mathbf{r}, \mathbf{r}_F(t)). \tag{1}$$

Here, t is the time and $\mathbf{r}$ and $\mathbf{r}_F(t)$ are 3-D vectors denoting image position and the position of the scatterer, respectively. The function h_F was then interpolated to a regular temporal grid using spline interpolation. The temporal resolution was chosen high enough to avoid aliasing of the signal for the highest velocities present while simultaneously being a multiple of the desired pulse repetition frequency (PRF).

C. Generating Multiple Scatterer Simulations

In this section, we describe how realizations with multiple scatterers were generated from a single scatterer realization. One simple way of achieving this is to regard the multiple scatterer realizations as a summation of several single scatterer signals with different amplitudes and time lags. In this case, the result may be written as a temporal convolution between h_F and a noise function n

$$s_F = n *_t h_F. \tag{2}$$

Each value $n(t)$ is a real-valued random variable with Gaussian distribution and represents the amplitude of scatterers with a time lag t. In the Fourier domain, this translates to

$$S_F(\mathbf{k}, f) = N(f)H_F(\mathbf{k}, f). \tag{3}$$

Note that it is important that the signal h_F does not contain aliasing before the noise filter, as this will lead to numerical errors.

In a flow-line realization, scatterers should be randomly and uniformly distributed within the entire spatial region associated with each flow line, as opposed to restricting their position to the central trajectory. To achieve this, scatterers were given a small random displacement parallel to the plane containing the seed points, with displacement magnitude less than or equal to the seed point grid size. In the Fourier domain, a spatial displacement $\mathbf{d}$ corresponds to multiplication by a phase factor with a frequency $\mathbf{k} \cdot \mathbf{d}$, where $\mathbf{k}$ is the wavenumber. In addition, if the displacement $\mathbf{d}$ is assumed to be small, the PSF can be assumed to be spatially invariant except for a phase shift proportional to $\mathbf{d} \cdot \mathbf{b}$, where $\mathbf{b}$ is a unit vector along the beam direction. A displacement of $\lambda/2$ along the beam should yield a phase shift of 2π radians. Incorporating these changes into (3) gives

$$S_F(\mathbf{k}, f) = N(f) \exp\left(2\pi i \left(\mathbf{k} + \frac{2}{\lambda}\mathbf{b}\right) \cdot \mathbf{d}(f)\right) H_F(\mathbf{k}, f). \tag{4}$$

Applying the inverse Fourier transform of $S_F(\mathbf{k}, f)$ produces the signal from a collection of point scatterers following the flow line F, as shown in the third column of Fig. 1. Then, the signal is downsampled to the desired PRF. One signal is generated for each flow line, and the resulting signals are added to produce a full realization, as shown in Fig. 1 (right). The process is repeated several times to produce multiple realizations, with functions n and $\mathbf{d}$ varying between flow lines and realizations. When generating realizations using multibeam acquisitions, the PSFs are calculated at the same positions and the functions n and $\mathbf{d}$ are the same for all transmitted beams.

III. METHODS

A. Investigated Velocity Estimators

1) Autocorrelation: To estimate mean velocity in the examples in this paper, the autocorrelation method [26] is used. If the complex beamformed in-phase/quadrature (IQ) signal from position $\mathbf{r}$ at transmission k is denoted $s(\mathbf{r}, k)$, the mean

phase shift between consecutive frames is calculated as

$$\Delta\phi(\mathbf{r}) = \angle\left(\frac{1}{N-1}\sum_{k=1}^{N-1}s(\mathbf{r},k)^*s(\mathbf{r},k+1)\right) \quad (5)$$

and converted to velocities using the relation

$$v(\mathbf{r}) = \frac{c\,\mathrm{PRF}\,\Delta\phi(\mathbf{r})}{4\pi f_c}. \quad (6)$$

Here, c is the speed of sound and f_c is the center frequency of the received signal.

2) PW Doppler: Estimates of the velocity distribution in each resolution cell are obtained using the modified periodogram [27]

$$S(\mathbf{r}, f) = \frac{1}{N}\sum_{k=1}^{N}w(k)s(\mathbf{r},k)\exp(2\pi i f_c k/\mathrm{PRF}) \quad (7)$$

where w is a window function used to suppress sidelobes in the frequency spectrum. Frequencies are converted to velocities using the relation

$$v = \frac{cf}{2f_c}. \quad (8)$$

3) 2-D Vector Doppler: The autocorrelation method only provides estimates of the velocity components in the beam direction. To produce vector velocity estimates, it is possible to combine the information from two or more beam directions using triangulation, or more generally, by solving a least squares problem [5], [6]. If v_m are the measured mean velocity components along the individual beam directions and v is the 2-D vector velocity, the least squares problem can be written as

$$\mathbf{A}v = \mathbf{v}_m \quad (9)$$

where A is a matrix projecting the velocities onto the beam directions with rows

$$a_n = [-\sin\alpha_n - \sin\beta_n, \cos\alpha_n + \cos\beta_n] \quad (10)$$

where α_n and β_n are the transmit and receive directions of the beam n. The problem posed in (9) has the solution

$$v = \mathbf{A}_W^\star v_m = (\mathbf{A}^T\mathbf{W}\mathbf{A})^{-1}\mathbf{A}^T\mathbf{W}v_m \quad (11)$$

where $\mathbf{A}_W^\star$ denotes the weighted Moore–Penrose pseudoinverse of $\mathbf{A}$. The matrix $\mathbf{W}$ contains weights that typically compensates for differences in variances between estimates from different angles.

4) 3-D Tracking Doppler: Tracking Doppler is a spectral velocity estimation technique in which the sample volume changes between different acquisitions, following scatterers with velocity v along a straight line [28], [29]. The signals from consecutive images are then summed, adding coherently for scatterers moving with the tracking velocity $\mathbf{v}$

$$\hat{p}(v) = \left|\sum_n w(n)s(\mathbf{r}+nv\Delta t\mathbf{e}_T, n_0+n)e^{-4\pi i f_c n v_z \Delta t/c}\right|^2. \quad (12)$$

Note that compared with conventional PW Doppler, tracking Doppler allows trading off spatial resolution for increased spectral resolution.

TABLE II
ACQUISITION AND PROCESSING SPECIFICATIONS

General		
Probe type	Linear array	Matrix probe
Transmit (Tx) freq. [MHz]	5	3
Pulse periods	4.5	3.5
Receive (Rx) F#	1.7	Full aperture
Apodization	Hamming	None
Beamforming region [cm]	2 x 1	2 x 1.5 x 2 cm
Beamforming grid resolution [mm]	0.2 x 0.1	0.7 x 0.7 x 0.2
Active transmit elements	192	60 x 48
Pitch [µm]	229	343
Azimuth F-number	1.5	Full aperture
Elevation aperture [mm]	6.5	16.5
Elevation Focus [mm]	35	Dynamic (Rx)
Doppler PRF [kHz]	10 (tube), 6 (carotid)	10 (coronary)
Ensemble size	64	64
Clutter filter:	5th order regression filter	
Vector Doppler 1 [deg]	Tx: [-15 15]	Rx: [-15] [15]
Vector Doppler 2 [deg]	Tx: [-15 15]	Rx:[-15 0] [0 15]

B. Beamforming

Conventional delay-and-sum beamforming was performed after IQ demodulation, using the UltraSound ToolBox (USTB) [30] with specifications found in Table II. In the particular case of the carotid bifurcation phantom, Fourier beamforming was applied. First, the channel data were beamformed using a full aperture. Then, the complex image data were filtered in 2-D Fourier space to produce data with the desired receive angle, F-number, and apodization. If $S(\mathbf{k}, t)$ is the 2-D spatial Fourier transform of the signal $s(\mathbf{r}, t)$, the filtering process can be written as

$$S_F(\mathbf{k}, t) = S(\mathbf{k}, t)\,w\left(\frac{\theta-\theta_0}{\arctan(1/(2F\#))}\right) \quad (13)$$

where $\mathbf{k} = [k_x, k_y, k_z]$, $\theta = \arctan(k_z/k_x)$, θ_0 is the receive angle, $F\#$ is the F-number, and w is the window function, defined to be 0 outside the interval $[-1, 1]$. The filtered signal s_F is obtained by inverse spatial Fourier transform of S_F. This approach is similar to [31], but using only one aperture instead of two. The motivation for using Fourier beamforming, in this case, was to avoid recalculating the PSFs in the cases where one transmit event has multiple receive events.

IV. SIMULATION SCENARIOS

The added value of FLUST compared with simulations based on randomly placed scatterers is demonstrated using three examples. As a first validation of the simulation technique, a straight vessel phantom and conventional Doppler velocity estimators are investigated. Then, the technique is applied to a patient-specific carotid bifurcation phantom to demonstrate how it can aid in the optimization of imaging setups for vector velocity estimation. Finally, we apply FLUST to 3-D Doppler imaging of a patient-specific model of a stenosed coronary artery, which facilitates a performance comparison of two spectral estimators for maximum velocity estimation.

A. Conventional Doppler Imaging in a Straight Vessel

A straight tube phantom with fully developed parabolic flow was simulated using both random scatterer (reference)
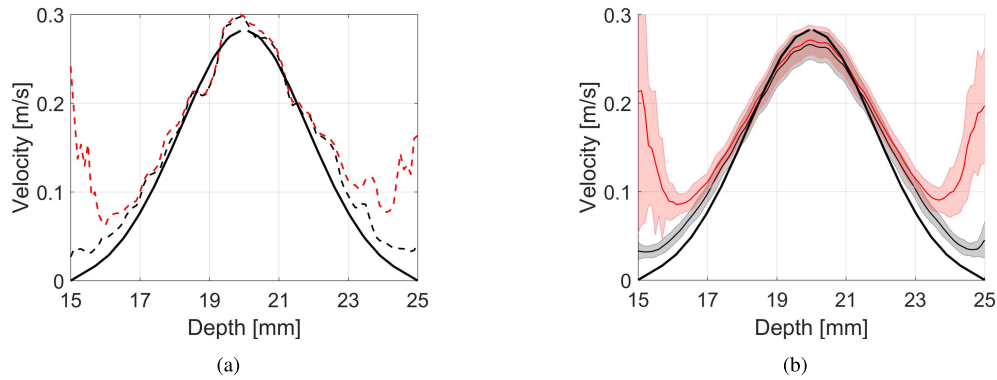
Fig. 2.   Velocity profiles in the straight vessel phantom. (a) Single realization using Field II. (b) Statistically expected velocity profile and standard deviation using 100 FLUST realizations shown in gray line (no clutter filter) and red line (with clutter filter), respectively. No spatial averaging is applied. The SNR is 30 dB and black thick lines show the true velocity profile in both figures.

and flow-line-based (FLUST) simulations. The tube had a diameter of 1 cm. A rectangular grid with a resolution 0.5 mm was positioned through a cross section, and all grid points inside the tube were selected as seed points. Flow lines were generated by forward and backward propagation as shown in Section II-A. The selected grid size resulted in 317 flow lines. The flow velocity in the middle of the tube was 0.56 m/s, and the beam-to-flow angle was 60°. This yielded a maximum velocity corresponding to 36% of the Nyquist velocity. An ensemble of plane-wave transmissions without steering from a linear array probe was simulated, with acquisition parameters described in Table II. After beamforming, random noise was added to the data with an SNR of 30 dB, to account for the thermal noise. The phantom contained no stationary clutter signal, but results were generated both with and without the application of a clutter filter, to assess the impact of filtering on accuracy and variance.

B. 2-D Vector Doppler Imaging in a Carotid Artery Bifurcation

As described in [32], a scatterer phantom was created based on fluid-structure interaction simulations of a patient-specific model of a stenosed carotid bifurcation. The phantom was positioned with the common carotid at a depth of 13 mm and with flow angles varying between 70° and 120° relative to the central beam direction. Field II simulations with random scatterer positions (reference) were performed as described in [33], whereas FLUST simulations were performed as described in Section III. The acquisition scheme consisted of plane-wave transmissions with steering angles −15° and 15° from a linear probe, transmitted with a firing rate of 12 kHz, but interleaved such that the Doppler PRF is 6 kHz for each angle. Two different receive setups were used to form two vector Doppler estimators (see Table II) which could be used in a performance comparison. For the reference simulation, the number of scatterers was about 80 000 per frame, corresponding to 10 scatterers per resolution cell. For each of the 64 frames, scatterers outside the imaging region were disregarded before performing calculations. When using FLUST, the PSF was calculated for about 160 000 scatterer positions distributed over 164 flow lines, evenly distributed through both branches.

For both simulation approaches, random noise was added to the data after beamforming, yielding an SNR of 30 dB.

C. 3-D Tracking Doppler in the Coronary Arteries

A coronary tree phantom was generated by first segmenting a computed tomography-scan from a patient with a stenotic left anterior descending coronary artery, using the Vascular Modeling Toolkit [34]. A steady-state solution was found for this geometry using the computational fluid dynamics software Fenics [35], with constant pressure at the inlet and constant resistance at the outlets. Flow lines were extracted from the solution, and translated and rotated so that the stenotic region was positioned at a depth 3.5 cm with a beam-to-flow angle of approximately 62°. Multiple realizations were generated as described in Section III. The acquisition was an ensemble of plane waves with a firing rate of 10 kHz without steering, from a 2-D matrix array. A PW Doppler sample volume was placed in the region containing the highest velocities. A tracking Doppler line was centered in the same sample volume, with orientation parallel to the flow lines going through the sample volume.

V. RESULTS

A. Motivational Example: The Straight Vessel Phantom

Using the previously described simulation and acquisition settings, a Field II simulation of a 64 frame Doppler ensemble takes 20 h in case of the straight vessel phantom. As shown in Fig. 2(a), autocorrelation over the ensemble may be used to obtain an estimate of the velocity profile normal to the vessel axis from a single realization. As seen from the dashed lines in Fig. 2(a), the velocity estimates have relatively high variance, motivating the use of spatial averaging. Spatial averaging would, in this case, cause a significant negative bias for the highest velocities and positive bias for the lowest velocities. Such spatial averaging effects can be avoided by simulating multiple realizations. In this case, 100 realizations of the flow field would require 2000 simulation hours using Field II.

In Fig. 2(b), 100 FLUST ensemble realizations have been used to obtain the expected autocorrelation velocity profile without the confounding effects of spatial averaging.
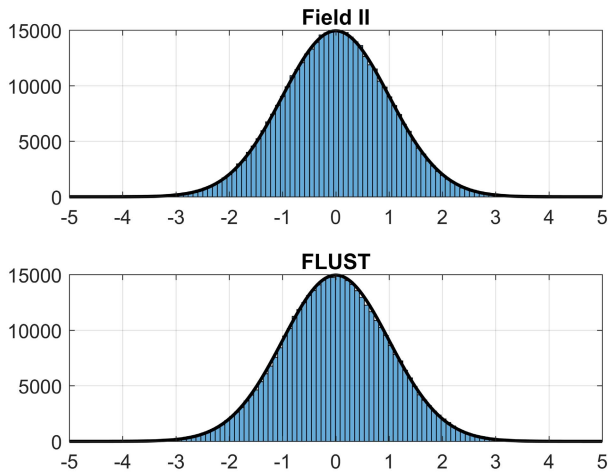
Fig. 3. Histograms of the real part of the simulated signal from one realization of the straight tube phantom. The black curve show a Gaussian distribution centered around 0 with standard deviation 1.

The total simulation time is 19 h, where 16 h are spent on creating the PSFs and 3 h are spent on generating multiple realizations. For this example, mean velocity and standard deviation are shown using gray lines (no clutter filter) and red lines (with clutter filter). The black thick line shows the true velocity. The impact of the spatial extent of the PSF can now be observed, yielding a small negative bias for the maximum velocities and a small positive bias for the low velocities close to the wall. If a clutter filter is applied, both the bias and variance close to the wall increase significantly.

B. Single Ensemble Validation

Fig. 3 shows the distribution of the real part of the IQ signal from one realization of the straight tube phantom. The values have been normalized to have a standard deviation of 1. As is seen, the signal distributions from Field II and FLUST both show good correspondence to the Gaussian distribution, indicating that the speckle is fully developed. The imaginary part of the signal shows the same good correspondence (data not shown).

Fig. 4 shows B-mode images (top) and spectral profiles (bottom) from the straight vessel phantom, using both the reference (Field II) and one ensemble realization of FLUST. The speckled appearance is similar, and they also show the same frequency spread for all depths.

Fig. 5 shows single B-mode images from FLUST and Field II simulations of the carotid bifurcation phantom, again demonstrating that the two simulation approaches yield similar speckle images. Fig.5 (bottom) shows the estimated vector velocities in the image plane, based on single realizations of the velocity field. The two approaches yield similar velocity magnitudes and directions. No spatial averaging is applied.

C. Application Example 1: Performance Evaluation of Two Alternative Vector Velocity Estimators

The FLUST method was used to obtain 100 ensemble realizations of the carotid bifurcation velocity field, which were
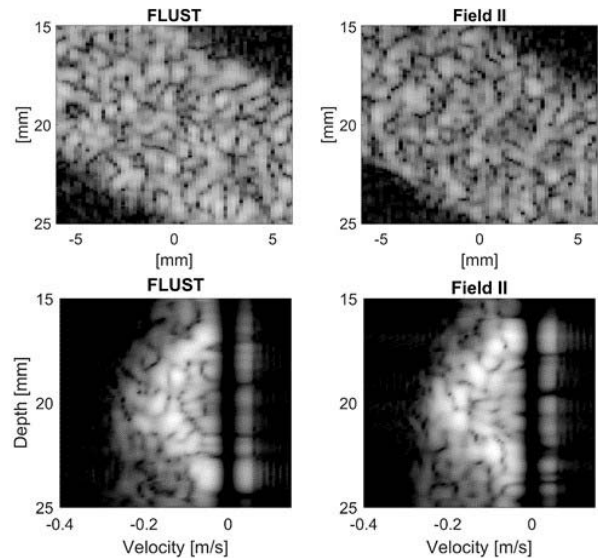

Fig. 4. Top: B-mode images from single realizations of the straight vessel phantom using the proposed technique (FLUST) and Field II. Bottom: corresponding spectral profiles based on single realizations (ensemble length = 64). Dynamic range is 50 dB.
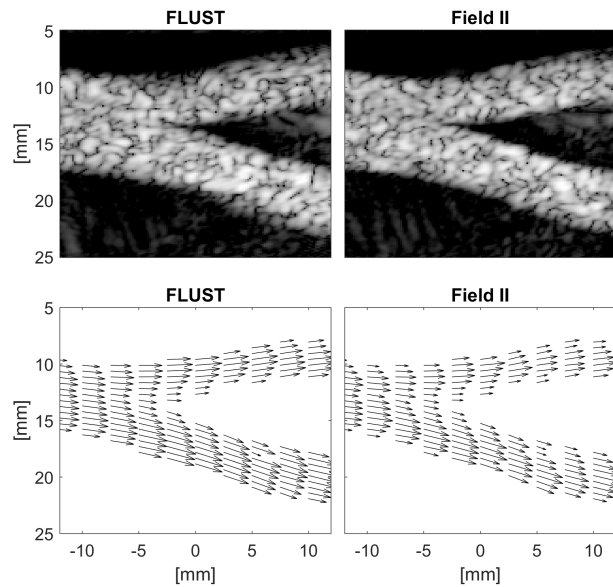

Fig. 5. Top: B-mode images from single realizations using the proposed technique (FLUST) and Field II. Dynamic range is 40 dB. Bottom: estimated vector velocity field based on single realizations of the velocity field (ensemble length = 64).

further used to compare the performance of two vector velocity estimators. The results are shown in Figs. 6 and 7. The total simulation time was 15 h, where 12 h were spent on creating the PSFs and 3 h on generating multiple realizations. As discussed further in Section V-E, 100 realizations of this velocity field would require 1700 simulation hours using Field II.

The vector velocity estimators are based on the same two-angle transmit sequence (see Table II) but have different receive settings; one yielding four unique Doppler measurements (top) and one yielding two Doppler measurements (bottom). Averaging the velocity field over all realizations enables direct comparison of the bias and variance of
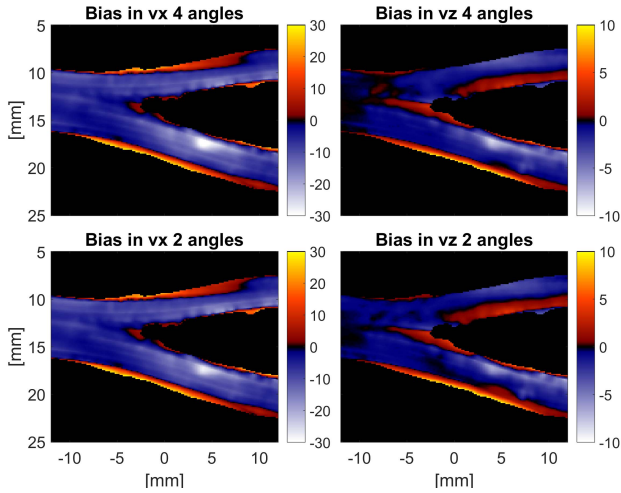
Fig. 6.   Velocity bias in each pixel using least squares vector Doppler with four angles and weighting (top) and dual-beam vector Doppler (bottom).
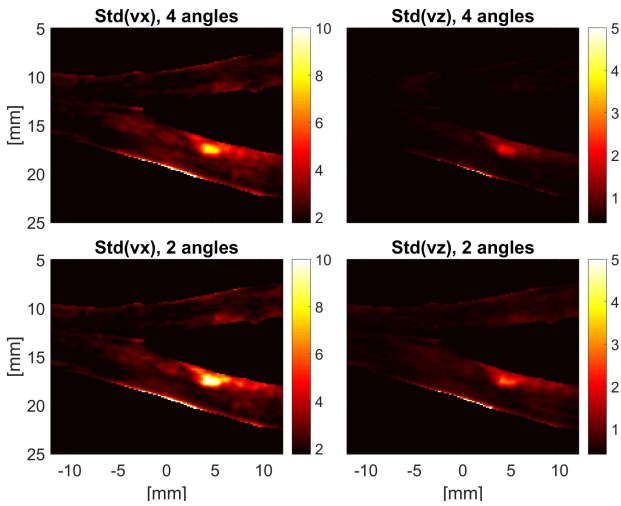

Fig. 7.   Standard deviation of the velocity estimates in each pixel using least squares vector Doppler with four angles and weighting (top) and dual-beam vector Doppler (bottom).

the two estimators in each image pixel. As can be seen in Figs. 6 and 7, the biases in v_x and v_z are similar for the two estimators, whereas the standard deviations are reduced in the four-angle case.

D. Application Example 2: Performance Evaluation of Two Maximum Velocity Estimators Used in 3-D Blood Flow Imaging of the Coronary Arteries

In Fig. 8(a), 100 flow-field realizations have been used to make a power Doppler isosurface (after clutter filtering) of the coronary artery phantom. The total simulation time using FLUST was 14 h (11 h for creating the PSFs and 3 h for generating multiple realizations). A corresponding simulation was not performed using the Field II software. The black ellipse indicates the location of the sample volume for PW Doppler and the central point of the tracking Doppler line.

The PW and tracking Doppler velocity spectra in Fig. 8(b) and (c) again demonstrate the added value of

having multiple realizations of complex flow fields available. Fig. 8(b) and (c) shows that using PW Doppler leads to increased spectral broadening compared with tracking Doppler, but the high variance in the velocity spectra in Fig. 8(b) hampers the quantification of spectral broadening and the determination of maximum velocities. Such measurements are, however, possible using the velocity spectra in Fig. 8(c), where 100 realizations are averaged. The velocity for which the power is −6 dB compared with the peak intensity measured at the descending slope at the highest velocities is termed the −6 dB velocity. The resulting −6 dB velocities were 2.88 and 2.56 m/s for PW Doppler and tracking Doppler, respectively. The true maximum velocity in the simulated coronary artery phantom was 2.47 m/s.

E. Computational Cost

Fig. 9 shows the calculation time for the carotid flow phantom as a function of the number of frames and realizations, using random scatterer-based and flow-line-based simulations. Field calculations were performed on a Quad Core 2.7-GHz Intel i7-6820HQ Processor using Field II pro version, whereas beamforming was performed on a NVIDIA Quadro M2000M GPU. The sampling frequency for the Field II calculations was 120 MHz. When using simulations based on randomly positioned scatterers, the computational load scales linearly with the number of frames and realizations simulated. For the example case with 64 frames, a flow-line resolution of 0.5 mm and a scatterer resolution of 0.05 mm along each flow line, the backscattered signal is calculated from a total of about 5 120 000 scatterers and the beamforming operation is performed 64 times. The total simulation time for one flow-field realization is about 17 h. On the other hand, the flow-line-based method first calculates the PSF for a total of 160 000 scatterer positions and performs the beamforming operation 160 000 times, using about 12 h. After this, 100 realizations of 64 frames each are generated using interpolation and application of noise filters, using about 3 h. The results show that using FLUST is faster than using scatterer-based simulations if the number of frames is larger than 48.

VI. DISCUSSION

A flow-line-based simulation method, termed FLUST, was proposed, and results using the new method were compared with simulations based on randomly positioned scatterers. The main advantage of FLUST is that, after some initial calculations, a large number of realizations of the same flow field may be generated at a low computational cost. The results indicated that realizations using FLUST are equivalent to those generated using conventional Field II simulations. Examples were shown from three different applications, in each case showing statistics from 100 realizations generated using FLUST, with total simulation time comparable to that of one single realization using conventional methods.

The two main parameters that determine the accuracy of FLUST are the density of calculated PSFs along each flow line and the density of flow lines. These parameters also determine the computational load because they implicitly determine the
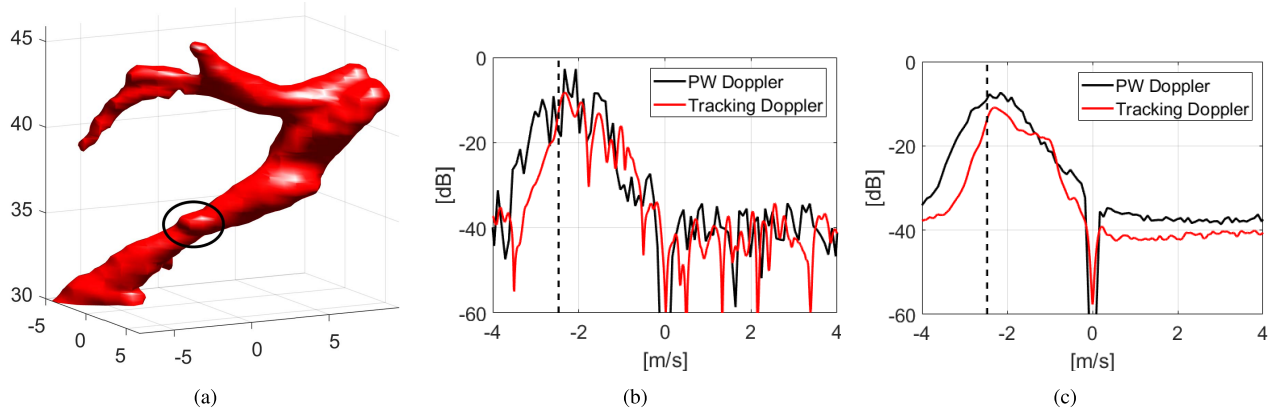
Fig. 8. (a) 3-D Power Doppler image of the coronary phantom, based on 100 realizations. Axes are in mm. The ellipse indicates the sample volume region for the spectral Doppler estimators. (b) PW and tracking Doppler spectra from a single realization of the flow field in the coronary phantom. (c) Expectation value/expected PW and Tracking Doppler spectra based on 100 realizations. The dotted line indicates the true peak velocity. The tracking direction corresponded to a beam-to-flow angle of $63.3°$, and an angle of $20.4°$ relative to the azimuth plane.
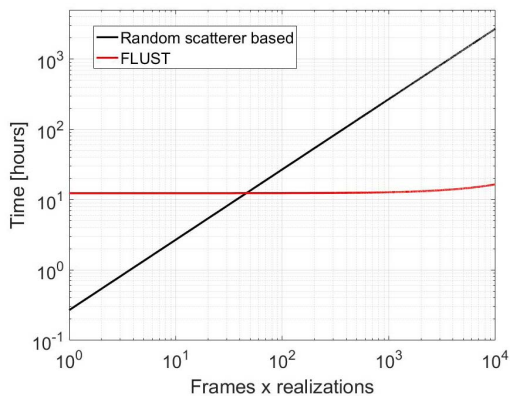

Fig. 9. Illustration of how simulation time scales with the number of realizations for the carotid flow phantom. Using the proposed FLUST method, it enables multiple realizations of complex flow fields with only a small increase in simulation time, whereas simulation time scales linearly with the number of frames and realizations for the random scatterer-based simulations. FLUST is the faster alternative when the total number of simulated frames exceeds 48.

total number of flow lines and calculated PSFs. The density of PSFs along each flow line influences the mismatch between scatterer-based simulations and FLUST due to the interpolation step when converting the PSFs to a temporal signal, as described in Section II-B. To minimize the interpolation error, spline interpolation is used and the PSFs are spaced with a distance of 0.05 mm along the flow line. In comparison, the examples in this paper use spatial wavelengths ranging from 0.3–0.5 mm. The spatial discretization of flow lines used in this paper was 0.5 mm. The underlying assumptions when selecting this discretization are that the observed velocity gradients are small and that the PSF is approximately spatially invariant for such displacements except for a phase factor. Figs. 2, 4, and 5 show both a good qualitative and quantitative correspondence between scatterer-based simulations and flow-line-based simulations, indicating that the chosen parameters yield sufficient accuracy for these applications. Note, however, that applications using higher center frequencies or with higher spatial velocity gradients might require smaller values for these parameters.

In order to estimate the statistical properties of velocity estimators, we need to use estimators that themselves often have high variance. This variance may in some cases be reduced by applying spatial averaging. In the presence of velocity gradients, however, the expectation value of the estimator will be dependent on the size of the averaging region. A too large averaging region will lead to a significant underestimation of maximum velocities and overestimation of velocities close to the vessel wall. Thus, accurately quantifying the bias and variance of estimators without spatial averaging effects necessitates the generation of several realizations of the same flow field. The results in Fig. 2 indicate that this may be achieved with low computational cost using the FLUST technique.

The results from applying autocorrelation-based vector Doppler to the carotid bifurcation phantom show a significant underestimation of velocities in the region with the highest velocities. No spatial averaging of autocorrelation estimates was performed in this case. The observed underestimation occurs because the spatial extent of the PSF covers a broad range of velocities. Similarly, a significant overestimation of velocities is seen close to the vessel walls. Notably, increasing the number of observation angles from 2 to 4 and using a weighted least-squares method did not lead to a reduction in these biases. It did, however, lead to a reduction in the variance of the estimator. One approach that might reduce the observed bias would be to reduce the pulselength or, in other ways reduce the spatial extent of the PSF. This, however, might yield increased variance. Again note that when using conventional Field II simulations, information about variance would not be available without producing several realizations, which would be more time-consuming.

The results from applying spectral estimators to the simulated coronary artery phantom illustrate the usefulness of having multiple realizations when comparing different spectral estimators. Even though the resulting spectra from one realization indicate that PW Doppler exhibit more spectral broadening than tracking Doppler, quantifying this property is difficult because of the high variance of both estimators. Averaging the spectra over several realizations reduces the

variance and makes the quantitative measures of broadening more reliable.

In the results presented in this paper, no clutter signal from surrounding tissues was present during simulations. Simulating tissue signal is not a straightforward using FLUST because when using this method it is implicitly assumed that the endpoints of flow lines are outside the insonation region. If FLUST had been used to simulate tissue lines with endpoints within the insonation region, scatterers would appear abruptly and discontinuously during simulations. Note that even without the presence of tissue signal, the results from FLUST may be used to compare the effect of clutter filters on the blood signal. The underlying assumption is that the clutter signal is negligible after filtering.

Another limitation of FLUST is that simulations are limited to stationary flow fields. As a consequence, any effects of acceleration will not be accounted for. It should be noted, however, that typical observation window lengths for ultrasound blood velocity estimators are smaller than 15 ms, for which it may be assumed that the effects of acceleration are negligible. But for applications with highly accelerated flow or longer temporal observation windows, this might be a source of inaccuracy.

The rapid generation of multiple realizations made available using flow-line-based simulations is useful in the development of velocity estimators. The ability to obtain reliable measures of the bias and variance of estimators is very useful for tuning setup parameters for a given estimator or for the comparison of different estimators. In this paper, examples were shown using Doppler-based mean estimators and spectral estimators, but further work includes using this tool to compare Doppler- and correlation-based estimators, e.g., speckle tracking [9], [36]. Also, in this paper, Field II was used to calculate PSFs, but depending on the application and required accuracy, FLUST could be combined with other simulation tools to further decrease simulation times. Finally, the FLUST method is inherently parallelizable, as both PSFs and different realizations are generated independently. Further parallelization of the method is, therefore, also a topic for further work.

VII. Conclusion

The FLUST method for simulation of stationary flow fields was proposed. Results show that realizations produced using FLUST correspond well with Field II simulations, both quantitatively and qualitatively. The runtime of FLUST is not significantly dependent on the number of simulated frames and realizations, and in the examples shown, it was the faster alternative once the total number of simulated frames exceeds 48. For the examples shown, the new simulation method is able to produce 100 realizations at the same time used to produce a single conventional Field II realization. This enables the estimation of statistical properties of velocity estimators with an accuracy that would be time-consuming to achieve using simulations based on random scatterer positions.

References

[1] W. A. Zoghbi *et al.*, "Recommendations for evaluation of the severity of native valvular regurgitation with two-dimensional and Doppler echocardiography," *J. Amer. Soc. Echocardiogr.*, vol. 16, no. 7, pp. 777–802, 2003. [Online]. Available: http://www.sciencedirect.com/science/article/pii/S0894731703003353

[2] B. Dunmire, K. W. Beach, K.-H. Labs, M. Plett, and D. E. Strandness, Jr., "Cross-beam vector Doppler ultrasound for angle-independent velocity measurements," *Ultrasound Med. Biol.*, vol. 26, no. 8, pp. 1213–1235, Oct. 2000.

[3] I. K. Ekroll, A. Swillens, P. Segers, T. Dahl, H. Torp, and L. Lovstakken, "Simultaneous quantification of flow and tissue velocities based on multi-angle plane wave imaging," *IEEE Trans. Ultrason., Ferroelectr., Freq. Control*, vol. 60, no. 4, pp. 727–738, Apr. 2013.

[4] S. Ricci, L. Bassi, and P. Tortoli, "Real-time vector velocity assessment through multigate Doppler and plane waves," *IEEE Trans. Ultrason., Ferroelectr., Freq. Control*, vol. 61, no. 2, pp. 314–324, Feb. 2014.

[5] B. Y. S. Yiu, S. S. M. Lai, and A. C. H. Yu, "Vector projectile imaging: Time-resolved dynamic visualization of complex flow patterns," *Ultrasound Med. Biol.*, vol. 40, no. 9, pp. 2295–2309, Sep. 2014. [Online]. Available: http://www.sciencedirect.com/science/article/pii/S0301562914001628

[6] I. K. Ekroll, J. Avdal, A. Swillens, H. Torp, and L. Løvstakken, "An extended least squares method for aliasing-resistant vector velocity estimation," *IEEE Trans. Ultrason., Ferroelectr., Freq. Control*, vol. 63, no. 11, pp. 1745–1757, Nov. 2016.

[7] J. A. Jensen and P. Munk, "A new method for estimation of velocity vectors," *IEEE Trans. Ultrason., Ferroelectr., Freq. Control*, vol. 45, no. 3, pp. 837–851, May 1998.

[8] M. Lenge, A. Ramalli, P. Tortoli, C. Cachard, and H. Liebgott, "Plane-wave transverse oscillation for high-frame-rate 2-D vector flow imaging," *IEEE Trans. Ultrason., Ferroelectr., Freq. Control*, vol. 62, no. 12, pp. 2126–2137, Dec. 2015.

[9] L. N. Bohs, B. J. Geiman, M. E. Anderson, S. C. Gebhart, and G. E. Trahey, "Speckle tracking for multi-dimensional flow estimation," *Ultrasonics*, vol. 38, nos. 1–8, pp. 369–375, Mar. 2000.

[10] J. A. Jensen and N. Oddershede, "Estimation of velocity vectors in synthetic aperture ultrasound imaging," *IEEE Trans. Med. Imag.*, vol. 25, no. 12, pp. 1637–1644, Dec. 2006.

[11] J. Udesen, F. Gran, K. L. Hansen, J. A. Jensen, C. Thomsen, and M. B. Nielsen, "High frame-rate blood vector velocity imaging using plane waves: Simulations and preliminary experiments," *IEEE Trans. Ultrason., Ferroelectr., Freq. Control*, vol. 55, no. 8, pp. 1729–1743, Aug. 2008.

[12] S. Fadnes, S. A. Nyrnes, H. Torp, and L. Lovstakken, "Shunt flow evaluation in congenital heart disease based on two-dimensional speckle tracking," *Ultrasound Med. Biol.*, vol. 40, no. 10, pp. 2379–2391, Oct. 2014.

[13] H. Takahashi, H. Hasegawa, and H. Kanai, "Echo speckle imaging of blood particles with high-frame-rate echocardiography," *Jpn. J. Appl. Phys.*, vol. 53, no. 7S, p. 07KF08, Jun. 2014.

[14] C. Tysoe and D. H. Evans, "Bias in mean frequency estimation of Doppler signals due to wall clutter filters," *Ultrasound Med. Biol.*, vol. 21, no. 5, pp. 671–677, 1995.

[15] J. A. Jensen, "Field: A program for simulating ultrasound systems," in *Proc. 10th Nordicbaltic Conf. Biomed. Imag.*, vol. 4, 1996, pp. 351–353.

[16] J. A. Jensen, "Simulation of advanced ultrasound systems using field II," in *Proc. IEEE Int. Symp. Biomed. Imag., Nano Macro*, Apr. 2004, pp. 636–639.

[17] J. M. Thijssen, "Ultrasonic speckle formation, analysis and processing applied to tissue characterization," *Pattern Recognit. Lett.*, vol. 24, nos. 4–5, pp. 659–675, Feb. 2003.

[18] A. Swillens, P. Segers, H. Torp, and L. Lovstakken, "Two-dimensional blood velocity estimation with ultrasound: Speckle tracking versus crossed-beam vector Doppler based on flow simulations in a carotid bifurcation model," *IEEE Trans. Ultrason., Ferroelectr., Freq. Control*, vol. 57, no. 2, pp. 327–339, Feb. 2010.

[19] J. Van Cauwenberge *et al.*, "Assessing the performance of ultrafast vector flow imaging in the neonatal heart via multiphysics modeling and *in vitro* experiments," *IEEE Trans. Ultrason., Ferroelectr., Freq. Control*, vol. 63, no. 11, pp. 1772–1785, Nov. 2016.

[20] T. Hergum, S. Langeland, E. W. Remme, and H. Torp, "Fast ultrasound imaging simulation in K-space," *IEEE Trans. Ultrason., Ferroelectr., Freq. Control*, vol. 56, no. 6, pp. 1159–1167, Jun. 2009.

[21] H. Gao *et al.*, "Hooge, "A fast convolution-based methodology to simulate 2-D/3-D cardiac ultrasound images," *IEEE Trans. Ultrason., Ferroelectr., Freq. Control*, vol. 56, no. 2, pp. 404–409, Feb. 2009.

[22] H. Gao, T. Hergum, H. Torp, and J. D'hooge, "Comparison of the performance of different tools for fast simulation of ultrasound data," *Ultrasonics*, vol. 52, no. 5, pp. 573–577, 2012.

[23] S. Storve and H. Torp, "Fast simulation of dynamic ultrasound images using the GPU," *IEEE Trans. Ultrason., Ferroelectr., Freq. Control*, vol. 64, no. 10, pp. 1465–1477, Oct. 2017.

[24] L. A. Aguilar, R. S. C. Cobbold, and D. A. Steinman, "Fast and mechanistic ultrasound simulation using a point source/receiver approach," *IEEE Trans. Ultrason., Ferroelectr., Freq. Control*, vol. 60, no. 11, pp. 2335–2346, Nov. 2013.

[25] L. Aguilar, J. Wong, D. A. Steinman, and R. S. C. Cobbold, "FAMUS II: A fast and mechanistic ultrasound simulator using an impulse response approach," *IEEE Trans. Ultrason., Ferroelectr., Freq. Control*, vol. 64, no. 2, pp. 362–373, Feb. 2017.

[26] C. Kasai, K. Namekawa, A. Koyano, and R. Omoto, "Real-time two-dimensional blood flow imaging using an autocorrelation technique," *IEEE Trans. Sonics Ultrason.*, vol. SU-32, no. 3, pp. 458–464, May 1985.

[27] P. D. Welch, "The use of fast Fourier transform for the estimation of power spectra: A method based on time averaging over short, modified periodograms," *IEEE Trans. Audio Electroacoust.*, vol. AU-15, no. 2, pp. 70–73, Jun. 1967.

[28] T. D. Fredriksen, I. K. Ekroll, L. Lovstakken, and H. Torp, "2-D tracking Doppler: A new method to limit spectral broadening in pulsed wave Doppler," *IEEE Trans. Ultrason., Ferroelectr., Freq. Control*, vol. 60, no. 9, pp. 1896–1905, Sep. 2013.

[29] T. D. Fredriksen, J. Avdal, I. K. Ekroll, T. Dahl, L. Lovstakken, and H. Torp, "Investigations of spectral resolution and angle dependency in a 2-D tracking Doppler method.," *IEEE Trans. Ultrason., Ferroelectr., Freq. Control*, vol. 61, no. 7, pp. 1161–1170, Jul. 2014.

[30] A. Rodriguez-Molares *et al.*, "The ultrasound toolbox," in *Proc. IEEE Int. Ultrason. Symp. (IUS)*, Sep. 2017, pp. 1–4.

[31] S. Salles, A. J. Y. Chee, D. Garcia, A. C. H. Yu, D. Vray, and H. Liebgott, "2-D arterial wall motion imaging using ultrafast ultrasound and transverse oscillations," *IEEE Trans. Ultrason., Ferroelectr., Freq. Control*, vol. 62, no. 6, pp. 1047–1058, Jun. 2015.

[32] A. Swillens, G. De Santis, J. Degroote, L. Lovstakken, J. Vierendeels, and P. Segers, "Accuracy of carotid strain estimates from ultrasonic wall tracking: A study based on multiphysics simulations and *in vivo* data," *IEEE Trans. Med. Imag.*, vol. 31, no. 1, pp. 131–139, Jan. 2012.

[33] J. Avdal, L. Løvstakken, H. Torp, and I. K. Ekroll, "Combined 2-D vector velocity imaging and tracking Doppler for improved vascular blood velocity quantification," *IEEE Trans. Ultrason., Ferroelectr., Freq. Control*, vol. 64, no. 12, pp. 1795–1804, Dec. 2017.

[34] L. Antiga, M. Piccinelli, L. Botti, B. Ene-Iordache, A. Remuzzi, and D. A. Steinman, "An image-based modeling framework for patient-specific computational hemodynamics," *Med. Biol. Eng. Comput.*, vol. 46, no. 11, p. 1097, 2008.

[35] M. Alnæs *et al.*, "The FEniCS project version 1.5," *Arch. Numer. Softw.*, vol. 3, no. 100, pp. 9–23, 2015.

[36] G. E. Trahey, J. W. Allison, and O. T. von Ramm, "Angle independent ultrasonic detection of blood flow," *IEEE Trans. Biomed. Eng.*, vol. BME-34, no. 12, pp. 965–967, Dec. 1987.

Jørgen Avdal (M'15) was born in Årdal, Norway, in 1984. He received the M.Sc. degree in industrial mathematics and the Ph.D. degree in medical technology from the Norwegian University of Science and Technology (NTNU), Trondheim, Norway, in 2009 and 2015, respectively.

He is currently a Post-Doctoral Researcher with the Department of Circulation and Medical Imaging, NTNU. His current research interests include blood flow imaging and spectral Doppler methods in diagnostic ultrasound.

Ingvild Kinn Ekroll was born in Ålesund, Norway, in 1984. She received the M.Sc. degree in biophysics and medical technology and the Ph.D. degree in medical technology from the Norwegian University of Science and Technology (NTNU), Trondheim, Norway, in 2009 and 2013, respectively.

She is currently a Researcher with the Department of Circulation and Medical Imaging, NTNU. Her current research interests include blood flow and tissue deformation imaging in diagnostic ultrasound.

Hans Torp (M'93) was born in Sarpsborg, Norway, in 1953. He received the M.S. and Dr.Techn. degrees from the Norwegian University of Science and Technology, Trondheim, Norway, in 1978 and 1992, respectively.

Since 1983, he has been a full-time Professor with the Department of Circulation and Medical Imaging, Faculty of Medicine, Norwegian University of Science and Technology. His research interests include stochastic signal/image processing with applications in ultrasonic imaging, Doppler, and color flow imaging.